TECHNICAL INFORMATION SERIES

R64SD67

SHOCK TUBE INSTRUMENTATION TECHNIQUES FOR STUDY OF HYPERVELOCITY ENTRY PROBLEMS

J.S. GRUSZCZYNSKI
D.A. ROGERS

SPACE SCIENCES LABORATORY

MISSILE AND SPACE DIVISION

GENERAL ELECTRIC

SPACE SCIENCES LABORATORY

EXPERIMENTAL FLUID PHYSICS SECTION

SHOCK TUBE INSTRUMENTATION TECHNIQUES FOR STUDY OF HYPERVELOCITY ENTRY PROBLEMS

By

J. S. Gruszczynski
D. A. Rogers

This work was partially supported by the Jet Propulsion Laboratory under JPL Contract 950297.

NAS 7-100

R64SD67
September 1964

MISSILE AND SPACE DIVISION

GENERAL ELECTRIC

CONTENTS

	PAGE
ABSTRACT	ii
INTRODUCTION	1
EXPERIMENTAL FACILITY	2
CURRENT AND VOLTAGE MEASUREMENT	3
TRIGGER GENERATION	5
SHOCK VELOCITY MEASUREMENT	6
TEST FLOW DETERMINATION	8
CONVECTIVE HEAT TRANSFER	11
RADIATION MEASUREMENTS	14
CONCLUDING REMARKS	19
ACKNOWLEDGEMENTS	21
NOMENCLATURE	22
REFERENCES	23

ABSTRACT

19757

The primary objective of this report is to describe shock tube instrumentation techniques developed especially for the study of convective heat transfer and the radiative properties of high temperature gases at conditions simulating hypervelocity entry into planetary atmospheres using an electrically heated helium driven shock tube. Techniques for overcoming the problem of very short test times (10 - 30 μ s) and electrical interference of the partially ionized test gas with the small signal from model heat transfer gages are presented and methods of evaluating test gas quality are described.

The measurement techniques described here have been applied to several studies of stagnation point convective heat transfer and radiative properties of high temperature gases. Typical results obtained in the course of these studies are shown and instrumentation requirements for the extension of aerothermodynamic investigation in the hypervelocity regime are outlined.

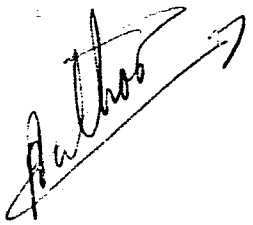

INTRODUCTION

The interest in space exploration has produced a need for further investigation of physical phenomena taking place in the gas flow around a space vehicle during its entry into various planetary atmospheres. In the development of such vehicles the design of the heat protection system is one of the most important problems. Because the useful payload capability is strongly dependent on the weight of such a system a precise knowledge of the magnitude of the heat transfer rates experienced by the vehicle is necessary. The projected flights to the near planets and during the return from a lunar mission will involve entry velocities equal to or higher than the orbital velocity. During re-entry from a suborbital flight, convective energy transfer from the high temperature shock layer across the boundary layer is the main source of heating. However, as the flight velocity increases, the radiative heat transfer becomes a significant fraction of the total heat transfer. For instance at the approximately 40,000 ft/sec velocity considered for entry into the atmosphere of the planet Venus, the radiation from the extremely high temperature gas in the shock layer will dominate the overall heating. Hence, both the convective and radiative heat transfer rates have been the subject of intensive experimental and theoretical investigations.

During the last three years much effort was spent on the development of facilities capable of simulation of the conditions corresponding to the hypervelocity environment encountered by the space vehicle during planetary atmospheric entry. Electrically heated helium driven shock tubes are able to

produce shock velocities at density levels required for proper reproduction of these flight conditions (1) (2). Because of the extreme pressures and temperatures present in such flows the measurement methods used in studies at moderate shock velocities had to be modified considerably and new techniques developed especially for the measurements of high temperature gas radiation. High shock velocities necessary for proper simulation of the thermochemical properties are associated with a very short duration, 10-30 microseconds, of the test flow in which the experiments are to be performed. This introduces a severe demand on the response of the instrumentation. Microsecond response of a gage is considered a prerequisite for its application in this type of hypervelocity research.

In the following sections of this paper, measurement techniques used in the General Electric Space Sciences Laboratory for studies of stagnation point convective heat transfer and high temperature gas radiance (3) (4) (5) will be described. Results of such studies can be meaningful only if the achievement of the desired level and steadiness of the flow properties is verified. Therefore, methods for measuring test time and the quality of the test flow are also discussed in detail.

EXPERIMENTAL FACILITY

The simulation of the orbital and superorbital enthalpies and pressures is accomplished in the arc heated shock tube illustrated in Figure 1. The ability of this shock tube to produce strong shock waves at relatively high initial pressures is obtained from the high temperature, high pressure, low molecular weight (helium) driver gas generated by a rapid discharge of

electrical energy stored in a capacitor bank. The driver is 3 in. in diameter and 4.5 ft. long. For most of the experiments which have been performed, the volume of the driver was reduced from the nominal dimensions by insertion of plastic spacers. A 304,000 (max) joule capacitor bank provides the energy for the driver gas heating. The driven tube is made of stainless steel. Its internal diameter is 6 in. and its overall length is 31.5 ft. The model stagnation point used for convective and radiative studies is located 2 ft. upstream from the end flange. Shock velocity up to 32,000 ft/sec was obtained with 1 mm Hg driven tube initial pressure using an 18 in. long driver and full energy in the capacitors. With a lower initial pressure and the same driver size, shock velocity up to 36,000 ft/sec was reached. By reducing the driver volume to approximately 17.5 in^3, a shock velocity of 43,500 ft/sec - equivalent to 59,000 ft/sec flight velocity - has been demonstrated.

Figure 2 shows the driven tube including instrumentation and associated equipment. A schematic diagram showing the shock tube instrumentation which was used in the experimental programs of convective and radiative heat transfer studies is presented in Figure 3. Also included in this diagram is the instrumentation necessary for the evaluation of the shock tube performance and for the determination of the quality of the test gas flow.

CURRENT AND VOLTAGE MEASUREMENT

Driver performance is monitored by measuring the discharge current and electrode voltage. The measurement circuits are shown in Figure 4a, which is also a schematic representation of the energy storage and discharge

system.

In order to avoid the problem of introducing a low inductance current shunt to measure the total discharge current, advantage is taken of the fact that the coaxial cable shields already provide a low resistance shunt. The capacitor bank consists of nineteen identical groups of sixteen capacitors each which are connected to the current collector assembly on the driver through equal lengths of RG-17/U coaxial cable. Thus, each cable carries very nearly 1/19 of the total discharge current. By carefully measuring the a-c resistance of a selected cable's shield return and monitoring the voltage drop from the capacitor bank end of it to ground (at the outer collector ring) a reasonably accurate measurement of the discharge current is obtained.

Electrode voltage is measured conventionally by means of a capacitance voltage divider having a total capacitance of about three picofarads and a ratio of about 1300 to 1. The larger capacitor is connected to the monitoring oscilloscope through a 10 Megohm attenuator probe in order to provide a time constant of about forty milliseconds.

Typical current and voltage waveforms are shown in Figure 4b for an arc chamber length of thirty inches and an initial capacitor bank voltage of 25.3 KV. The damped oscillations on the current waveform are attributed to a small amount of dissimilarity in the impedance parameters of the nineteen groups of capacitors which results in some circulating current between the groups.

TRIGGER GENERATION

To obtain proper triggering of the instrumentation oscilloscopes, the output of pressure sensors upstream of the event to be monitored are used. The step in pressure associated with the arrival of the shock is readily predictable, and the pressure gages used (Swiss Locomotive and Machine Works Type PZ-14) have proven extremely long-lived and reliable whereas thin film heat gages were considered unsatisfactory for this application because they would have to be replaced after each test. The major disadvantages of these pressure gages are their rise time of approximately seven microseconds and their response to vibration which may result from sound propagated down the wall of the driven tube due to operation of the driver and the diaphragm opening. Also, since piezoelectric gages are high impedance devices, they are susceptible to voltage pickup from the electric arc discharge.

The trigger circuit developed for use in the G. E. Space Sciences Laboratory shock tube and tunnel facilities is shown in Fig. 5. The pressure gage is connected to a variable gain amplifier which has a frequency response from about 200 cps to about 150 kcs. A band-reject filter at the amplifier output is used to eliminate triggering due to mechanical resonance of the gage at its natural frequency of about 48 kcs. The output from the filter is coupled to the control grid of a Type 5727/2D21 miniature hydrogen thyratron which is biased just below cut-off. The thyratron shield grid is used as a gating grid, being normally biased to prevent ionization until a time after all

spurious signals due to the capacitor bank discharge have died out. At this time - nominally about 600 microseconds after initiation of the driver discharge - a positive gate is applied to the shield grid which brings it to essentially zero bias and enables the thyratron to ionize on arrival of the shock at the pressure gage. The thyratron anode voltage step is differentiated to produce a low impedance, high amplitude oscilloscope trigger. Values of load resistance are selected to allow the tube to continue to conduct until reset manually, thus assuring only a single trigger.

Calibration of the triggering systems is accomplished by applying a step voltage about a factor of five smaller than the expected gage voltage signal to the amplifier input and adjusting the gain to give triggering when a gate is applied. The system has been used with generally good reliability for test conditions in which the pressure step across the shock was as low as 1.5 psi.

SHOCK VELOCITY MEASUREMENT

In order to monitor accurately the relative time of arrival of the shock at various stations along the tube, a raster type of oscilloscope display is used in which the time base is provided by a linear triangular waveform, unblanking is provided by the internal oscilloscope circuits, and vertical deflection is obtained by adding the oscilloscope sweep sawtooth at the pre-amplifier input to the shock time of arrival signals. Accurate time marks obtained from the crystal controlled triangle generator at a rate ten times the frequency of the triangle are applied to the cathode-ray tube cathode to

intensity modulate the trace.

Time of arrival signals are obtained by differentiating and adding the output of photomultipliers located at various stations along the tube sidewall. The photomultipliers are mounted in holders which attach to the tube and which contain a pair of collimating slits to restrict the viewing angle of the photomultipliers, thus assuring a fast leading edge in the output pulse. A block diagram of the raster system and a typical raster record are shown in Figures 6a and 6b respectively. Some of the PM outputs are inverted before display in order to assure correct identifications of their location. The arrival of the shock front at each station can be read with an accuracy of about $\pm 0.5\ \mu$ sec which, for example, at shock velocity of 30,000 ft/sec gives an accuracy of better than 2%.

A second method of measuring shock velocity, which has been used as a backup for the raster display, uses the output of two sidewall piezoelectric pressure gages. The gages are located a known distance apart and are connected through cathode followers to the two inputs of a Tektronix Type C-A preamplifier. The preamplifier is set to add the two signals algebraically, to amplify the signal from the downstream gage by about a factor of five more than that of the upstream gage, and to invert the signal from the upstream gage. Sweep speed is calibrated before the test by means of a crystal controlled time mark generator. Figure 6c shows the results of this type of measurement on a dual beam oscilloscope so that shock velocity between two pairs of stations could be obtained on the same display. The

ringing of the gages is superimposed on their pressure response; however, it does not interfere with the accurate determination of the shock arrival time.

Typical shock speed data obtained from the raster display is shown in Fig. 7. For comparison, data from the pressure gage arrangement is also shown. A good agreement between these two methods is evident.

TEST FLOW DETERMINATION

In the simulation of superorbital velocities in the shock tube a great concern is the available test time as determined by the length of the shock processed gas between the incident shock wave and the passage of the interface region separating the gas initially in the driven tube and the driver gas. It was found that the actual test time is much shorter than the prediction calculated on the basis of viscous flow but neglecting turbulent mixing caused by the finite opening time of the diaphragm. Also, it was found that the available test time can differ from run to run although the test conditions are kept the same. Measurements taken in a hypervelocity shock tube demand proper recognition of the test time during each experimental run. Various techniques have been used. These are shown in Figs. 8a through 8e. Two of these techniques are photometric.

In the first one the emitted light from the shock heated gas behind the incident shock wave is observed. The traces from a multichannel monochromator with each channel covering a fairly narrow band of the spectrum are shown in Fig. 8a. The arrival of the shock front is associated with a

sudden appearance of strong radiation overshoot which decays to an equilibrium level within a short time, as the gas relaxes to the thermo-chemical equilibrium and its temperature drops. The uniform level of emitted energy corresponding to the test gas flow follows until the contact zone arrives, at which moment the test time ends. The emission from the gas is a very strong function of its temperature. Hence, the steadiness of the test gas emission is a good indication of its quality. It is interesting to note that, depending on the wavelength, the end of the test time is indicated either by a rise or a decrease of the emitted radiation. It was also observed that under some conditions of shock velocity and pressure, there is no sharp boundary defining the end of the test time for certain wavelengths. This implies that, if this method is used for defining the test flow, more than one region of the spectrum should be monitored.

Using a two channel photometer, the quality and the length of the test time and the length of time necessary to establish steady flow around the model is determined by monitoring the emission from the shock layer ahead of the stagnation point of the hemispherical model. This method is necessary whenever model experiments are performed. In the present studies the red channel covered a spectral range from 5000 to 12000 $\mathring{A}$ while the blue channel was sensitive to radiation between 3500 and 4800 $\mathring{A}$. Oscilloscope traces of the signals from the two channel photometers are shown in Fig. 8b. The upper trace corresponds to the blue channel and the lower trace is from the red channel. The steadiness of shock layer intensity determines the quality

of stagnation region flow. In most cases the blue signal shows an increase in intensity upon the arrival of the mixed gas in the contact zone while the red channel indicates a drop in radiation at its response wavelength. On some occasions, however, as in the case of the incident wave observations, one of the channels may show no change in the intensity level at the end of the test time, confirming the need for more than one wavelength channel to properly identify the test time.

An image converter camera was also used to assess the quality of the flow by showing the shape of the incident shock wave and the symmetry of the model flow. This is illustrated in Fig. 8c where a photograph obtained with a 0.050 μ sec exposure and containing three frames, taken 10 μ sec apart, is shown.

During the convective heat transfer measurements, the potential of the calorimeter gage with respect to ground can be used for defining the length of the test time. A typical trace is shown in Fig. 8d, where the arrival of the contact zone is clearly indicated by the appearance of noise. A somewhat less precise method, mainly due to a low temporal resolution, was the time resolved spectrography. A spectrogram of the stagnation region gas is shown in Fig. 8e. From our experience during the experimentation in the hypervelocity shock tube, we have concluded that the test time determination should not be based on a single technique and that the results obtained from more than one method should be cross-checked for consistency before accepting the experimental data as absolutely valid.

CONVECTIVE HEAT TRANSFER

The measurements of stagnation point convective heat transfer rates in the hypervelocity flight regime have been made using two techniques. The first one uses a calorimeter type gage (6). The second depends on surface temperature history measurements using thin film thermometry (7). Both of these methods are capable of microsecond response, a prerequisite for hypervelocity shock tube application. The internal construction of the calorimeter heat transfer gage is shown in Fig. 9a. A metallic element (platinum, gold or nickel) 0.002 in. thick, 1/16 in. wide and 1/4 in. long serves as the calorimeter. To avoid disturbance of the flow in the boundary layer the gage is recessed forming a continuous surface with the insulating epoxy plug. A photograph of a $R_N = 0.5$ in. stagnation point heat transfer model is shown in Fig. 9b. Metal and phenolic nylon models were used in order to determine whether any electrical effects due to conductance of the model could be affecting the gage response but no difference in the response was observed. The gage was connected to a battery through a relatively large resistance (approximately 4 Ω) so that a constant current flows through the gage during the test. A change of resistance due to the change of temperature caused by the heat flow to the gage produces a voltage signal which can be related to the heat transfer rate by

$$\dot{q} = \frac{\rho c \ell}{\alpha E_o} \frac{dE}{dt}$$

If the heat flux is steady, the signal is a straight line with a constant slope.

During the initial stages of convective heat transfer studies in the hypervelocity shock tube the calorimeter gage signals were found to have several undesirable characteristics. The potential of the gage with respect to ground showed a strong negative signal, which normally reached about 5-7 volts just prior to the arrival of the incident shock wave at the model, at which time the potential would jump to approximately 2 volts positive as shown in Fig. 10a.

Arrival of the shock-produced plasma at the gage results in a common mode signal equal to this potential. The differential amplifier used for extracting the few millivolt heating signal must be capable of rejecting this common mode signal. Thus, to obtain accurate measurement of the change in gage voltage due to heating, it is necessary to carefully balance the measuring system before a test. A calorimeter gage signal with an insufficient balance is shown in Fig. 10b.

The technique used for making differential balance adjustments is illustrated in Fig. 11a. With the gage mounted in the model and the circuit connected as it would be during the test, a positive pulse simulating the plasma induced potential is applied to the exposed surface of the gage element and the amplifier (a Tektronix Type "D" Preamplifier) differential balance controls are adjusted for a minimum residual signal on the oscilloscope. Traces showing input and output signals are presented in Fig. 11b. Low frequency rejection of at least 80 db is readily obtainable; however, differences in phase and frequency response within the preamplifier limit the high frequency rejection to about 70 db. This high frequency residue is limited to about

3-5 microseconds which is about the time required for the flow about the model to become established during the test. In addition to the careful balancing, proper shielding of the leads and accurate circuit symmetry are required for protection against disturbances caused by electromagnetic coupling. With these precautions applied, a clean signal from the calorimeter gage was obtained. Typical traces at two different shock velocities are shown in Fig. 11c.

Because of the high heating rates and short test times associated with the hypervelocity heat transfer measurements in the shock tube, the use of gage response in which the heat is assumed to be distributed uniformly across the gage thickness will be in error. Time dependent temperature distributions and hence the correction for this effect in the case of platinum gages has been calculated. As can be seen from Fig. 12 the correction for thinner gages is small; however, a thin gage will lose heat to its backing material early in the test time. Therefore, we have selected a 0.002 in. thickness as the most appropriate for the platinum gage.

The thin film convective heat transfer gage is shown in Fig. 13a. A platinum film is deposited on a quartz, semi-spherical plug which in turn is mounted at the stagnation point of the model. The response of the gage to heat flux is governed by the following expression

$$\dot{q}(t) = \frac{\sqrt{\pi\, K_2\, \rho_2\, C_2}}{\alpha\, E_o} \left\{ \frac{E(t)}{2\sqrt{t}} + \frac{1}{2\pi\sqrt{t}} \int_o^t \frac{\sqrt{\lambda}\, E(t) - \sqrt{t}\, E(\lambda)}{(t-\lambda)^{3/2}}\, d\lambda \right\}$$

This equation was programmed for the IBM 7090 computer and upon integration gives time histories of the heat flux corresponding to the photographic oscilloscope records. Because of the extreme conditions of heat transfer rates, 20,000 Btu/ft^2-sec and higher, involved in the hypervelocity studies, the application of the thin film gages is limited. The surface temperature of the substrate rises during the test, changing the characteristic thermal diffusivity which enters into the data reduction equation. This parameter not only becomes a function of time but also a function of distance from the surface. As shown in Ref. 8 large corrections for this effect are necessary, increasing the uncertainty of the heat transfer rate data. Response of a stagnation point thin film heat transfer gage is shown in the upper trace of Fig. 13b. The lower trace is the red channel of the two color photometer viewing the shock layer ahead of the stagnation point. In this particular case a correction of 21% was applied to compensate for the changing properties of the substrate.

RADIATION MEASUREMENTS

The study of high temperature gas radiation requires a measuring device which is able to sense total radiance, integrated over the whole spectrum from several hundred Angstroms to several microns. As the gas temperatures of interest increase it can be expected that more and more of the total emitted radiant energy will be located in the UV region of the spectrum. All photo-emitting devices such as photomultipliers, phototubes, etc. are sensitive only to a limited range of wavelength. A thin film resistance gage (7) of a type widely used in shock tubes and shock tunnels

for measuring convective heat transfer would be suitable due to its high sensitivity and fast response. However, a difficulty arises in the determination of the surface reflectivity which in most cases is a function of the surface conditions, the wavelength of the incident radiation and the incident angle. In practical application the surface conditions are difficult to control and there is a lack of a suitable calibration system for reflectivity calibration below 2000 $\mathring{A}$, a wavelength region important in the studies of high temperature gas radiation. Also there is always a possibility that the optical properties of the gage surface can change during a test run.

The gage described here draws on the black body principle for its geometric shape as is shown schematically in Fig. 14a. The gage is made in the form of a cylindrical body with the entrance slit set off-axis. The interior of the gage is coated with a thin film of platinum which serves as a fast response resistance thermometer. The radiant energy which enters through the slit is partially absorbed by the platinum film and partially reflected. Because of the chosen geometry the photons will undergo several reflections before they escape back through the entrance slit. However, due to a finite absorption on each incidence, less than 5% of the energy entering the cavity gage will escape if the absorptivity of the platinum film remains higher than 30%. Fast thermal response of the gage is dependent on the film thickness which should be made small relative to the characteristic thermal diffusion depth of the film material. At the same time the film must be made opaque to the incident radiation since its function is to absorb the

energy. The transmission of thin, sputtered platinum films was therefore investigated. The results indicate that a film of about 0.1 micron thickness transmits less than 1% of the incident energy in the wavelength range between 0.2 and 1.0 micron. Its transmission becomes even less for shorter wavelengths.

During initial operation of the gage, signs of photoemission were experienced. During runs where the gage was evacuated to a pressure of approximately 3 microns the photoelectric effect was strong enough to make the potential of the gage become negative. A few runs were made with a glass window under the same flow conditions with no evidence of the photoelectric effect, indicating that the photons with energy corresponding to a wavelength smaller than 3500 Å are required to cause the photoemission. To eliminate this effect the gage was filled with pure nitrogen at 1 atm pressure. The presence of nitrogen gas reduced the mean free path of the electrons, building up a space charge close to the surface of the gage within a fraction of a microsecond, thereby inhibiting any further electron emission. Nitrogen gas was chosen because of the high energies required for photodissociation and photo-attachment.

The thin film resistance thermometer, the sensor of the cavity gage, is operated at constant current in a circuit shown in Fig. 14c. Each lead is connected through a 1500 ohm resistor to a dry cell battery bank. The gage leads are connected to the inputs of a differential amplifier in order to reject any noise pick up in the gage circuit.

Two experimental configurations were employed. In the first configuration, the measurements are made of radiation emitted from gas processed by the incident shock wave. This arrangement is shown in Fig. 15a. The gage was located behind a set of collimating slits viewing only a narrow layer of the gas across the shock tube. In all recent investigations a fused silica quartz window separated the gage from the radiating gas. The space around the gage was filled with pure nitrogen at 1 atm pressure. The geometry of the radiating volume is indicated by the limiting rays in Fig. 15a. In reducing the data to energy per unit solid angle per unit volume, the total radiating volume contributing radiant energy to the gage was calculated and an effective value corresponding to the parallelpiped extended by the entrance slit computed.

Because of the limited temperatures and densities in the incident shock flow which can be produced at a given initial shock tube pressure with the available energy of the driver, the gas radiance at temperatures in the range of 12,000-16,000°K was measured using the stagnation region gas ahead of a hemispherical model. This arrangement of the total radiation cavity gage inside the model is shown in Fig. 15b. A rectangular shaped sapphire window 0.1 in. by 0.5 in. and 1 mm thick was used at the stagnation point of the model. The gage itself is located away from the window with its entrance slit parallel to the window aperture. Thus, the gage senses only radiation from a region of the shock layer close to the axis of the model.

It was found that the flow establishes quickly after the passage of the incident shock wave and remains relatively steady for a sufficiently long time

to permit the measurements of the energy emitted by the shock layer. Difficulties were experienced with models having a nose radius larger than 1.0 in. Since it is desirable to have the shock stand-off distance as large as possible, attempts were made to use models with R_n = 1.5 in. and 2 in. with 3.0 in. diameter cylindrical afterbody. No satisfactory data could be obtained, mainly due to the difficulty of establishing a steady flow around the model as indicated by large fluctuations of the red and blue channel photometer signals. The R_n = 1.0 in. model did not experience this unsteadiness and the test flow was found to be reasonably uniform.

Typical traces obtained at three different flow conditions with the above described cavity gage are shown in Fig. 16. The approximate parabolic signal of the cavity gage (upper trace) is typical of the response of a thin film thermometer gage to an approximately constant heating rate. The steadiness and duration of the test flow in the radiating shock layer can be seen from the traces (lower trace) of the photometer observing the stagnation region gas. The corresponding history of the stagnation gas radiance, as obtained by the reduction of the cavity gage voltage signal from the previous figure, is shown in Fig. 17.

Before the readings obtained from the cavity gage can be interpreted in terms of the radiative power emitted by the stagnation region gas one must know the radiating volume and the steradiancy of the emitters. The radiating volume is defined by the field of view of the gage entrance slit and

the model window aperture. The depth of the radiating volume extended from the model surface to the bow shock wave. This dimension depends on the flow conditions - initial shock tube pressure and shock velocity - and were measured by two techniques. Entrance slits of two photometers were focused on the axis of the model ahead of the stagnation point at a distance encompassing the expected location of the bow shock. The character of the signal from these instruments indicated whether the predicted location was correct. A more accurate measurement was made using an STL image converter camera. The results were found to agree with the theoretical predictions of Serbin (10).

CONCLUDING REMARKS

Calorimeter heat transfer gages have been adapted to the study of stagnation point convective heat transfer in the hypervelocity shock tube. A total radiation gage was developed and its application to the measurement of high temperature gas radiance demonstrated. Because of the need to extend radiation measurements into the spectral region below 2000 $\mathring{A}$, a windowless version of the cavity gage is being developed.

Model pressure measurements should be made using small pressure gages with fast (microsecond) rise time. To preserve the fast response characteristic, the gages would have to be flush mounted and would as a consequence be exposed to very large surface temperature rise during the test time. This should not affect their response. The other highly desirable characteristic of these gages would be a minimum acceleration sensitivity

in order to eliminate the effects of model vibration and acceleration. At the present time, this last requirement appears to be the most difficult to satisfy, since standard quartz crystal piezoelectric gages are available which appear capable of meeting the other requirements.

It would seem that much valuable data such as temperature, electron concentration, etc. could be obtained from time resolved spectrograms taken behind the incident shock and in the model flow. Efforts to use the streaking mode of the STL Image Converter Camera in conjunction with a fast spectrograph look promising in this regard.

A special purpose analog computer for the measurement of shock velocity and generation of a pulse with a correct delay to trigger downstream instrumentation has been designed. It should greatly reduce the number of tests during which valuable data is lost because the predicted shock velocity was not attained. This is especially a problem when total sweep durations of ten or twenty microseconds are desired for good time resolution.

ACKNOWLEDGEMENTS

The authors wish to express their indebtedness to Dr. W. R. Warren for many helpful discussions and to Miss B. Maguire who operated the experimental instrumentation.

NOMENCLATURE

D	diameter
E	voltage, energy
I	intensity
L	length
P	pressure
R	radius
T	temperature
U	velocity
V	voltage
c	specific heat
k	thermal conductivity
l	thickness
q	heat transfer
t	time
x	coordinate
α	temperature coefficient of resistivity
λ	variable of integration, wavelength
ρ	density

Subscripts

1	initial driven tube
2	behind incident shock, substrate
f	flight
i	initial
m	model
o	standard conditions, initial
r	radiative
s	shock
D	driver
N	nose (model)

REFERENCES

1. Warren, W.R., Rogers, D.A., and Harris, C.J.; The Development of an Electrically Heated Shock Driven Test Facility; 2nd Symp. on Hypervelocity Techniques, Univ. of Denver, Denver, Colorado; March, 1962. Also GE-MSD Doc. No. R62SD37; April, 1962.

2. Camm, J.; Escape Velocity Shock Tube With Arc Heated Driver; 2nd Symp. on Hypervelocity Techniques, Univ. of Denver, Denver, Colo.; March, 1962.

3. Gruszczynski, J.S., Warren, W.R.; Measurements of Hypervelocity Stagnation Point Heat Transfer in Simulated Planetary Atmospheres; GE MSD Doc. No. R63SD29; March, 1963.

4. Gruszczynski, J.S., Warren, W.R.; Experimental Heat Transfer Studies of Hypervelocity Flight in Planetary Atmospheres; to appear in AIAA J., September, 1964.

5. Gruszczynski, J.S., Warren, W.R., and Diaconis, N.S.; Laboratory Simulation of Hypervelocity Heat Transfer Problem during Planetary Entry; to be presented at the XVth International Astronautical Congress, Warsaw, September, 1964.

6. Rose, P.H.; Development of the Calorimeter Heat Transfer Gage for Use in Shock Tubes; Rev. Sci. Inst. 29, 557-564, (July, 1958).

7. Vidal, R.J.; Model Instrumentation Techniques for Heat Transfer and Force Measurements in a Hypersonic Shock Tunnel; Cornell Aero. Lab. Rept. No. AD-917-A-1, February, 1956.

8. Hartunian, R.A. and Varwig, R.L.; A Correction to the Thin Film Heat Transfer Measurements; Aerospace Corp. Rept. No. TDR-594 (1217-01) TN-2; May, 1961.

9. Gruszczynski, J.S., Harris, C.J., Rogers, D.A. and Warren, W.R.; Fast Response Total Radiation Gage for Measurement of Radiant Emission from High Temperature Gas; IEEE Paper No. CP 63-438, January, 1963. Also GE-MSD Doc. No. R63SD11; January, 1963.

10. Serbin, H.; Supersonic Flow Around Blunt Bodies; JAS 25, No. 1; January, 1958.

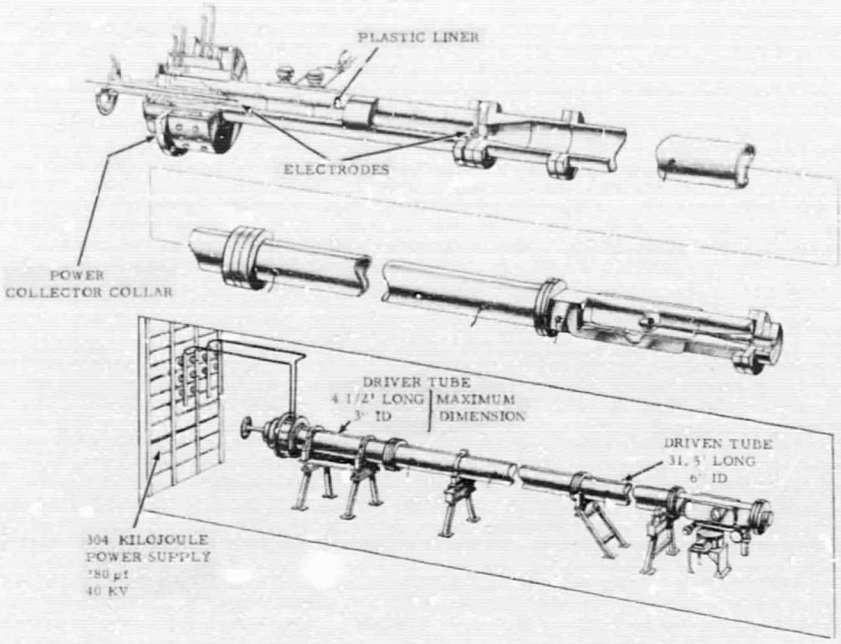

Figure 1. Hypervelocity Shock Tube with Electrically Heated Helium Driver.

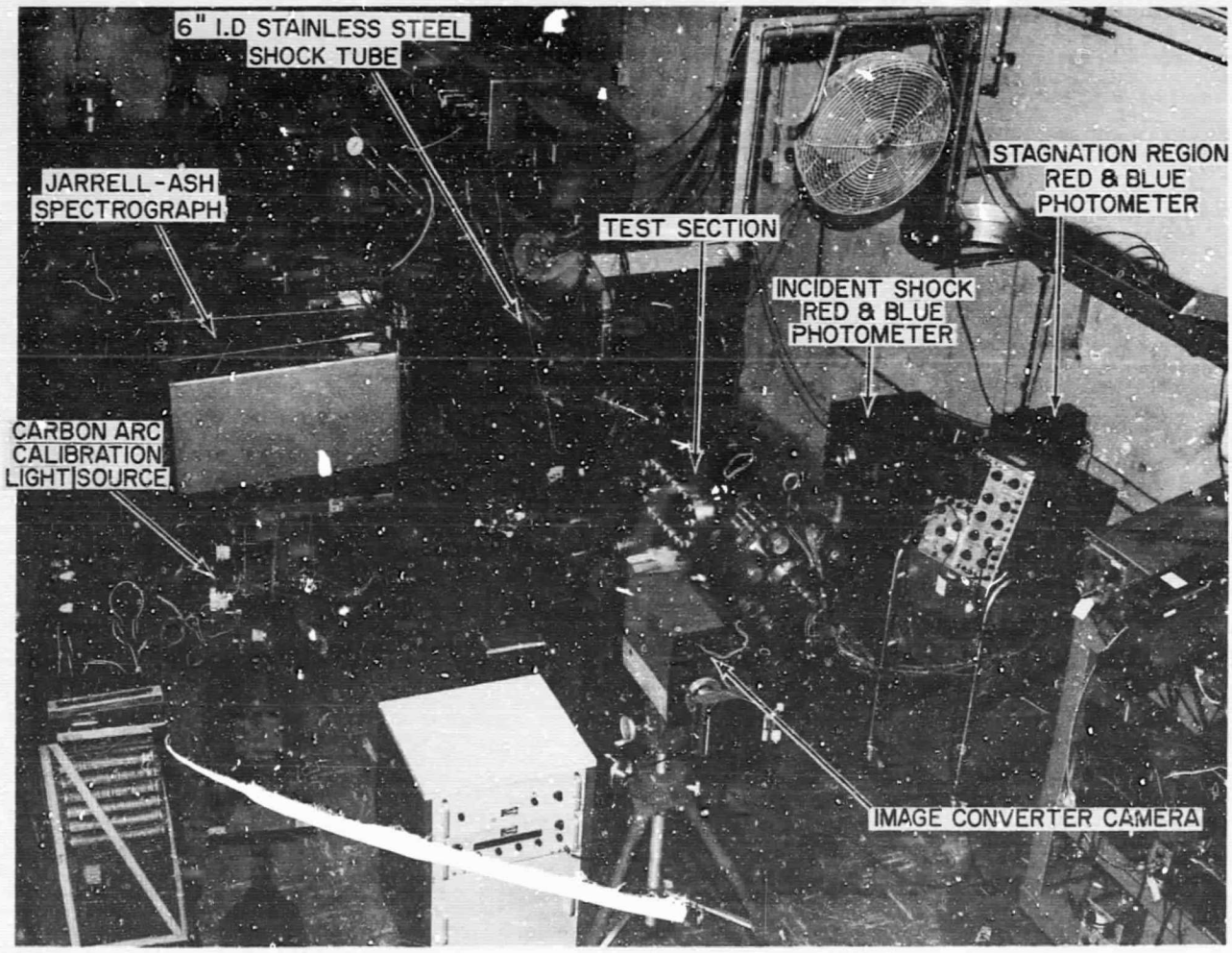

Figure 2. Driven Tube Including Test Section and Instrumentation.

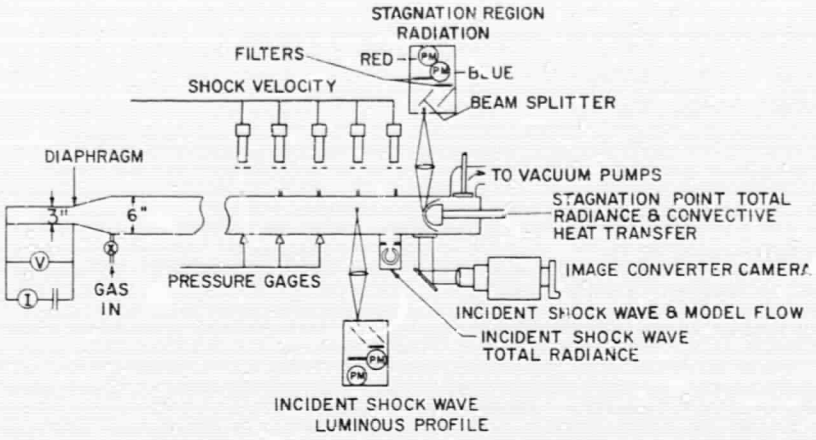

Figure 3. Schematic Diagram of Instrumentation for Convective and Radiative Heat Transfer Studies.

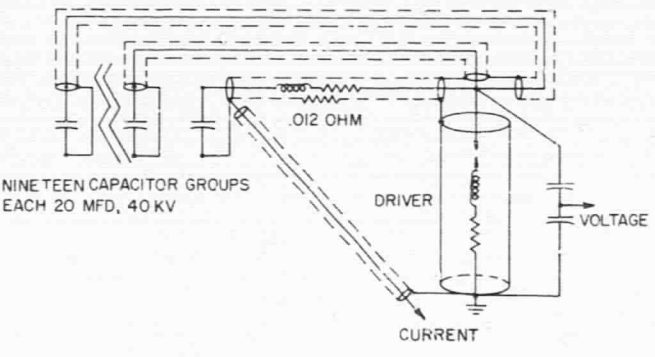

igure 4a. Schematic Diagram of Energy Storage and Discharge System.

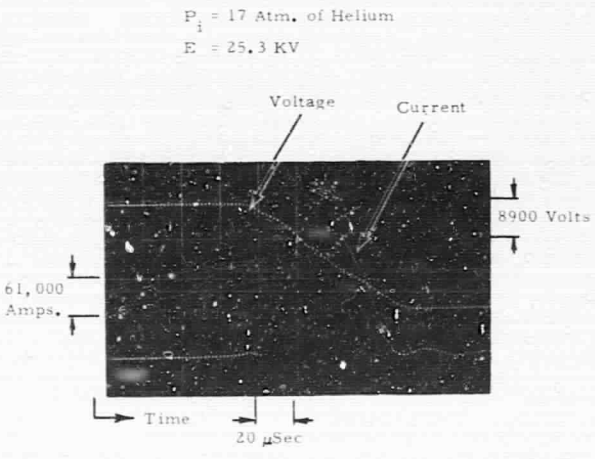

Discharge Current and Electrode Voltage

Figure 4b. Oscilloscope Traces of Discharge Current and Electrode Voltage.

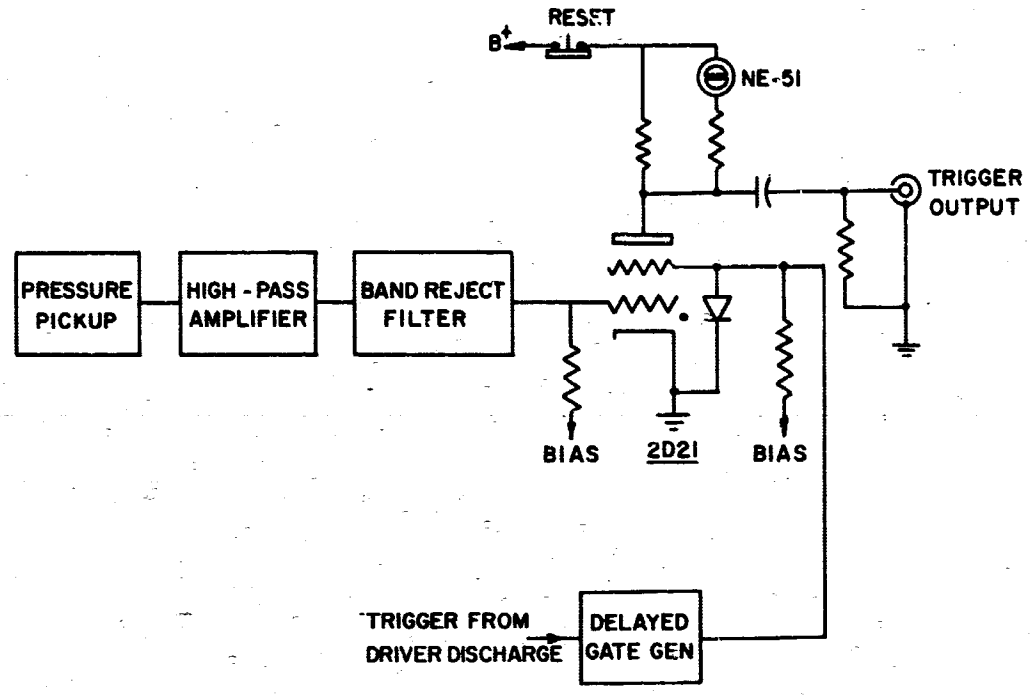

Figure 5. Schematic Diagram of Scope Trigger Circuit.

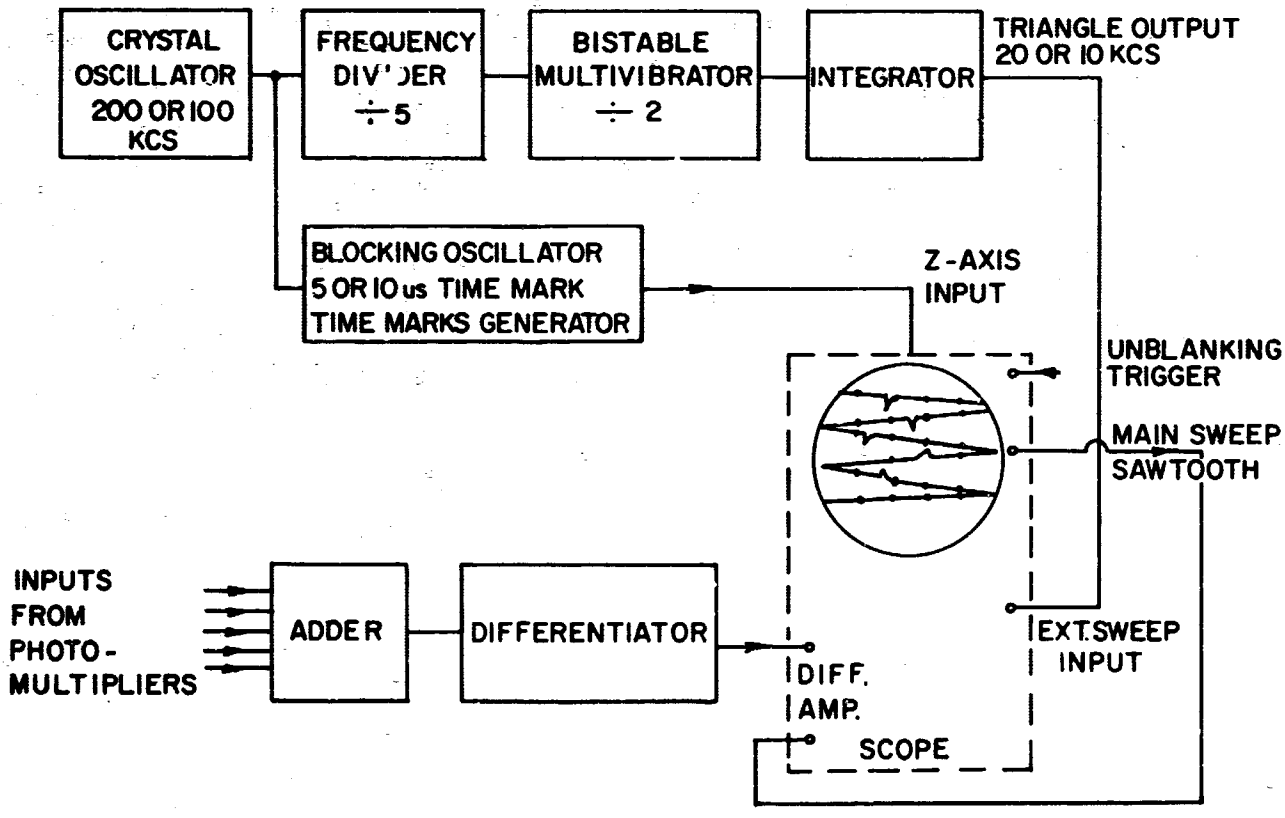

Figure 6a. Schematic Diagram of Raster Generator.

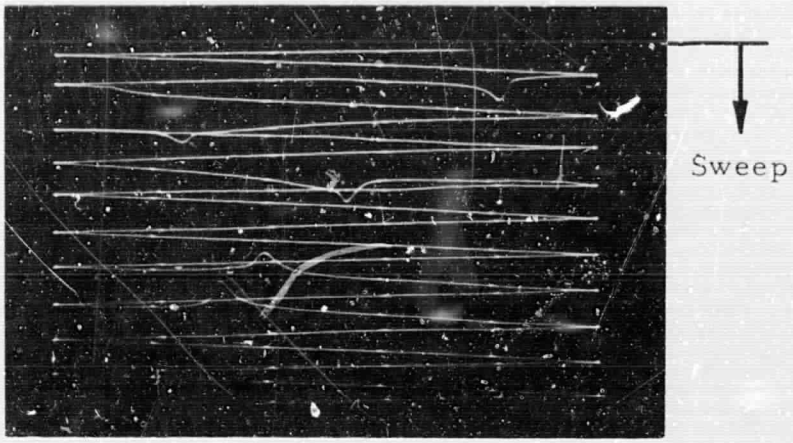

P_1 = 0.1 mm Hg U_s = 26,200 Ft/sec

Crystal Oscillator Markers 5 μsec Apart

Figure 6b. Oscilloscope Trace of Raster with Differentiated Photomultiplier Signals Indicating Passage of the Incident Shock Front.

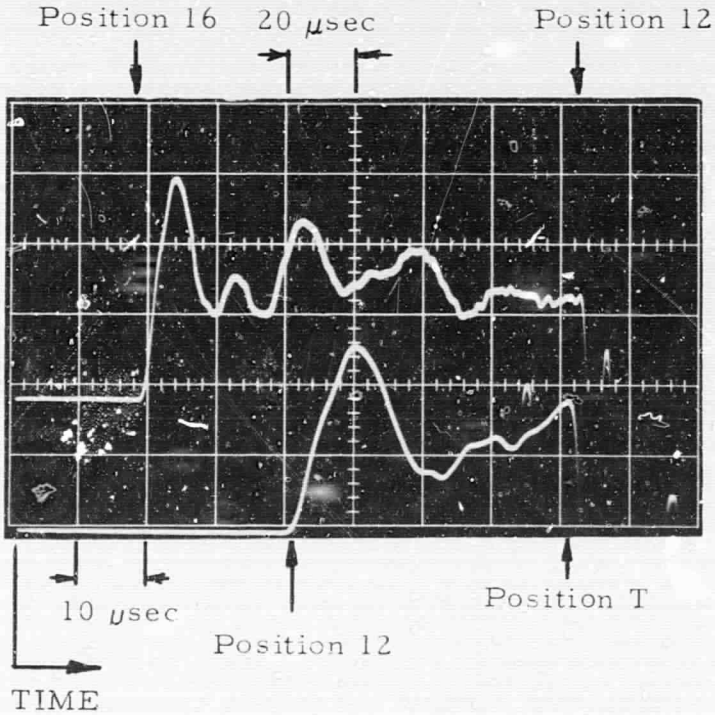

P_1 = 1.0 mm Hg U_s = 30,000 Ft/sec

Figure 6c. Oscilloscope Trace of Pressure Gage Signals from Two Consecutive Stations. Second Signal Inverted with Higher Amplifier Gain.

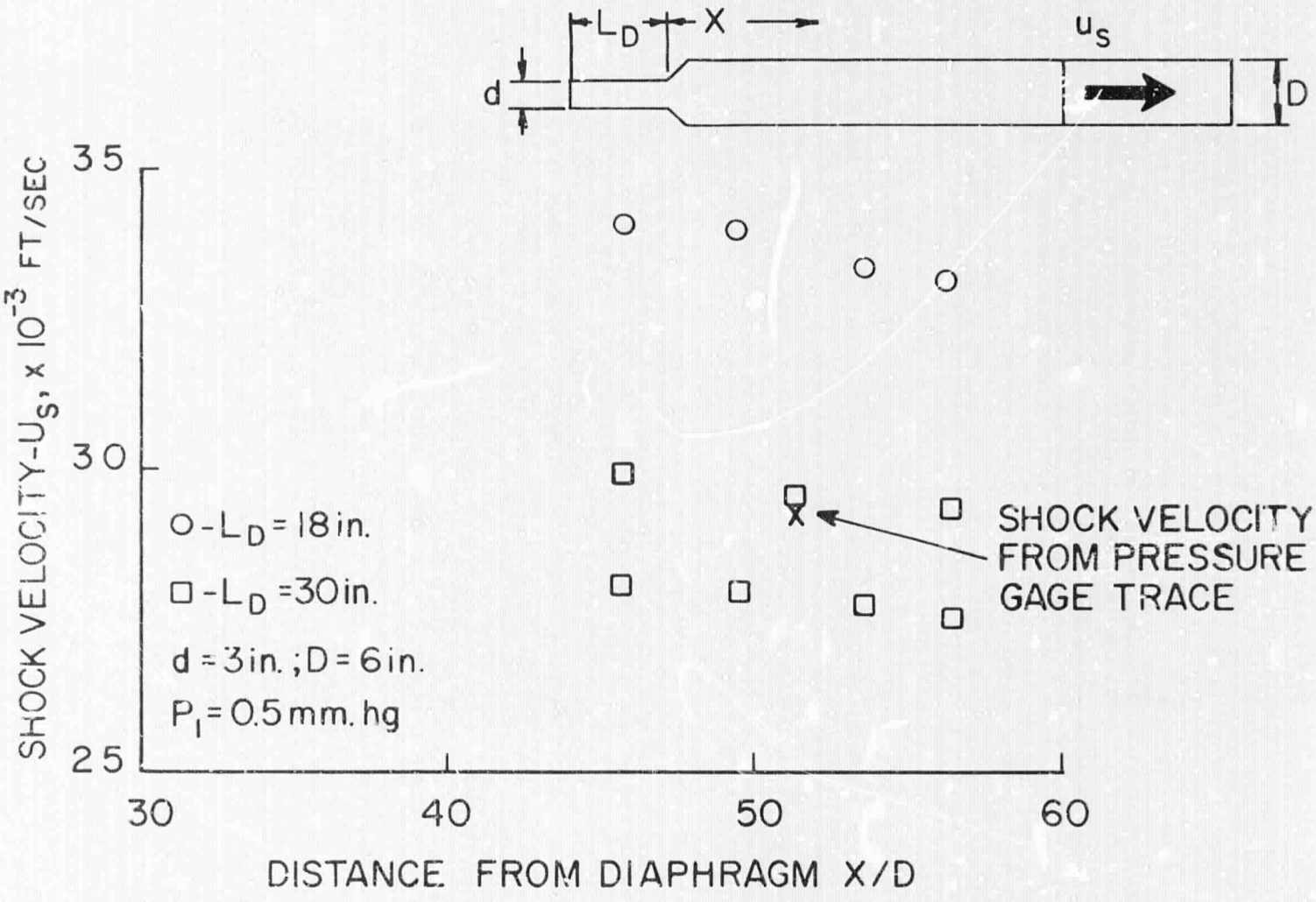

Figure 7. Shock Velocity Variation Along the Shock Tube.

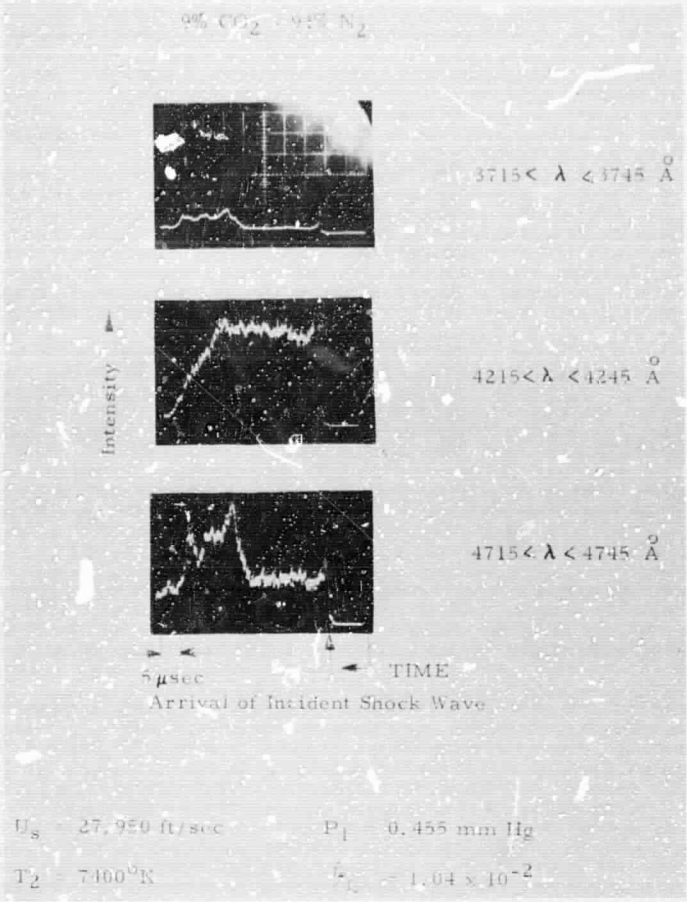

Figure 8a. Oscilloscope Traces of Radiation from Incident Shock.

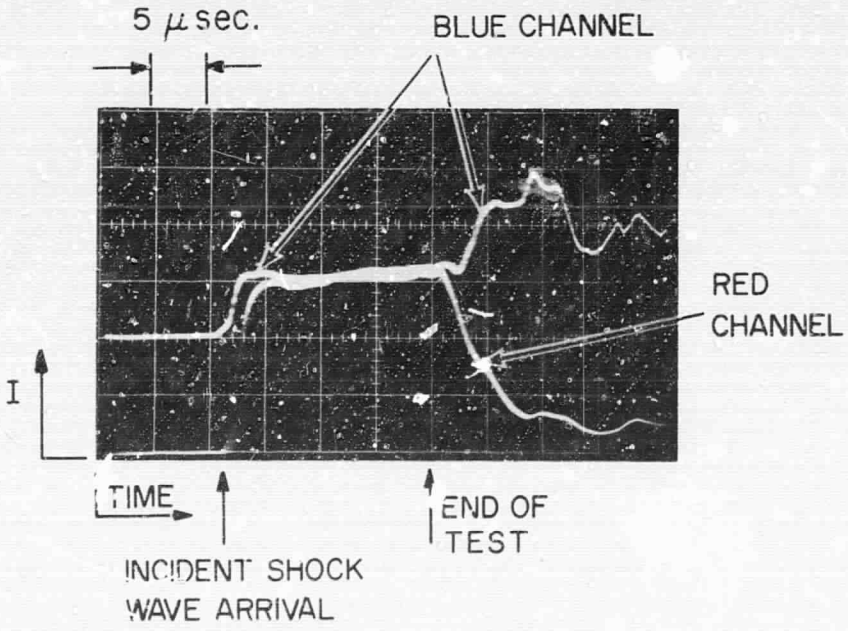

u_s = 28,000 FT./SEC. P_1 = 0.5 mm Hg

Figure 8b. Oscilloscope Traces from Two Color Photometer Viewing Stagnation Region Ahead of the Model. Top Trace Shows Blue Channel (3500-4800 Å). Bottom Trace Red Channel (5800-12000 Å).

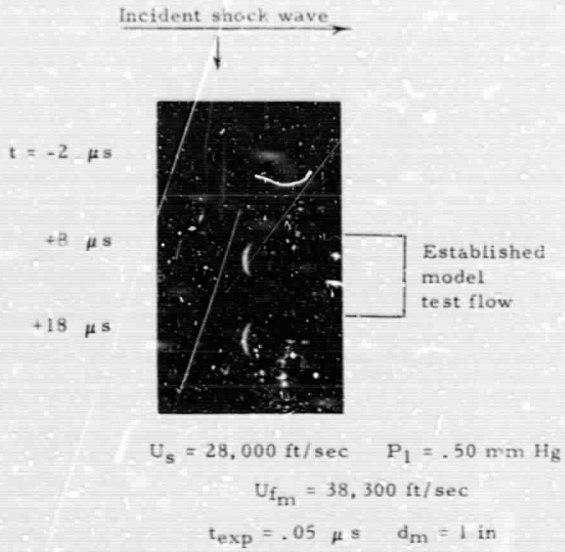

Figure 8c. Image Converter Camera Photograph of Incident Shock Wave and Model Flow. The Three Frames are 10 μ sec Apart. Top Frame Shows Incident Shock Approaching Model. Middle and Bottom Frames Show Established Flow Around a Hemispherical Model.

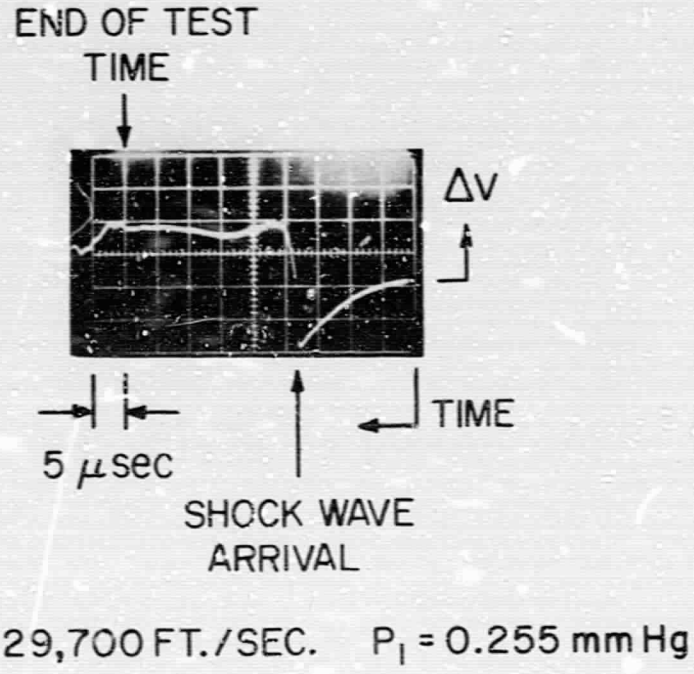

Figure 8d. Oscilloscope Trace of the Potential Level of a Calorimeter Gage with Respect to Ground.

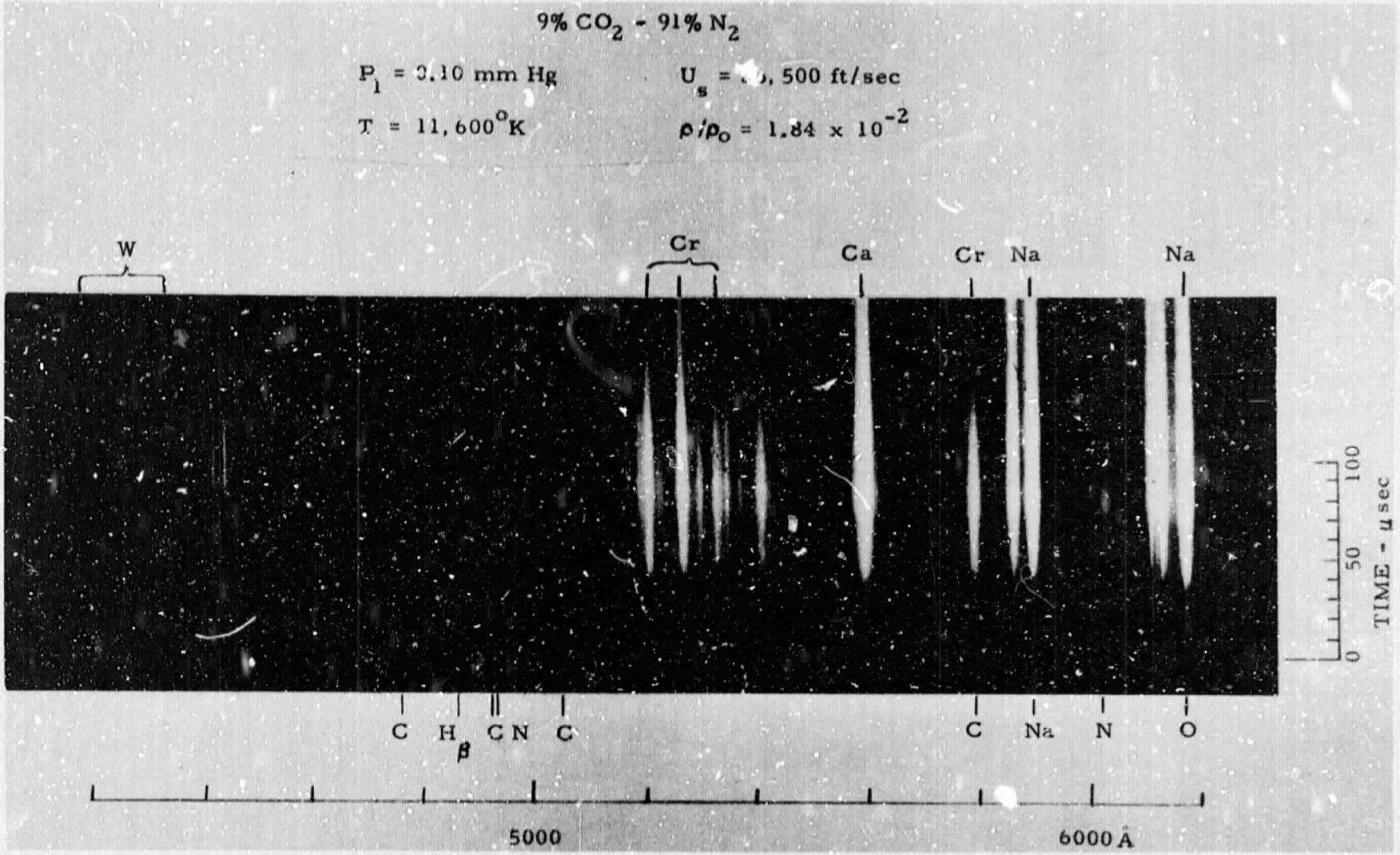

Figure 8e. Time Resolved Spectrogram of Gas in the Stagnation Region of Hemispherical Model. Instrument has f/3.5 Glass Optics and Time Resolution of 11 Microseconds.

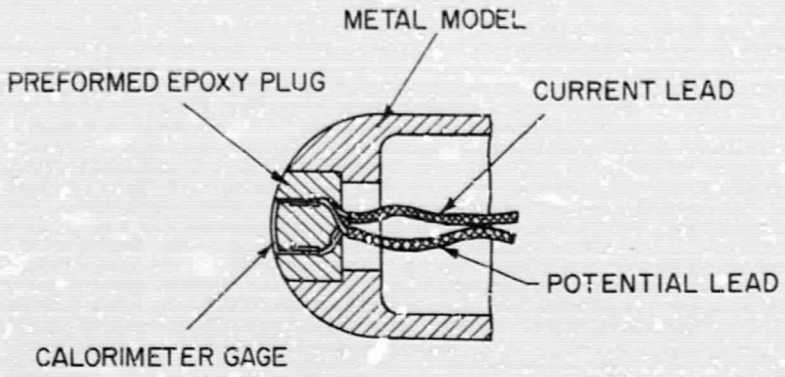

Figure 9a. Construction Detail of Calorimeter Heat Transfer Gage.

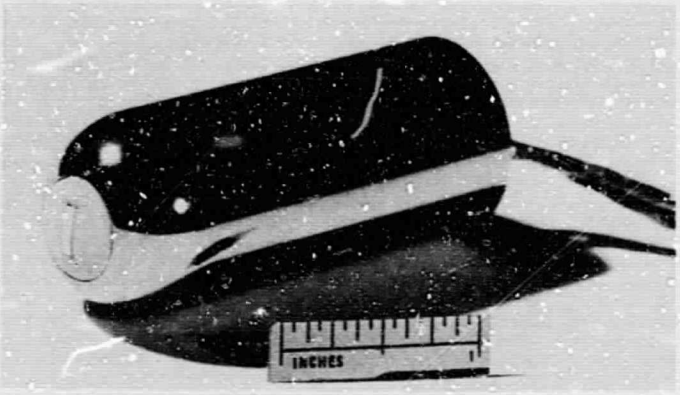

Figure 9b. Photograph of Calorimeter Gage Model. Model R_N = 0.5 in.

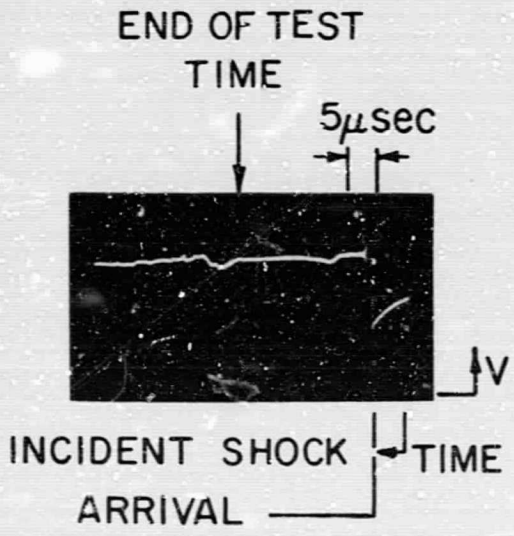

Figure 10a. Potential Level of the Calorimeter Gage with Respect to Ground.

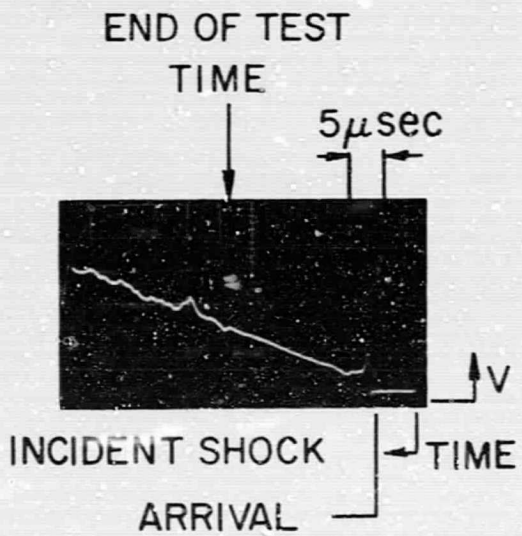

25 % CO_2 - 75 % N_2

Figure 10b. Oscilloscope Trace of Stagnation Point Calorimeter Gage Signal. Insufficient Preamplifier Balance is Evident.

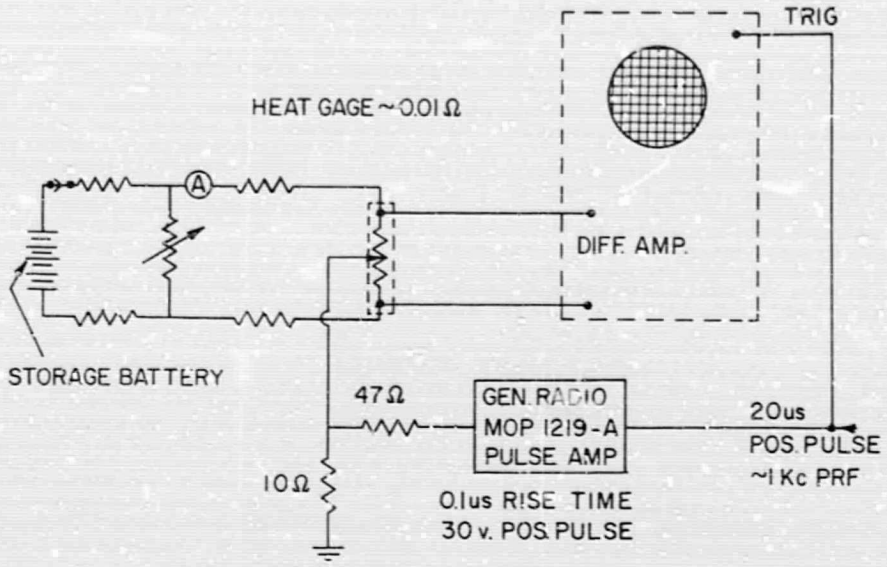

Figure 11a. Schematic Diagram of Calorimeter Gage Balancing Technique.

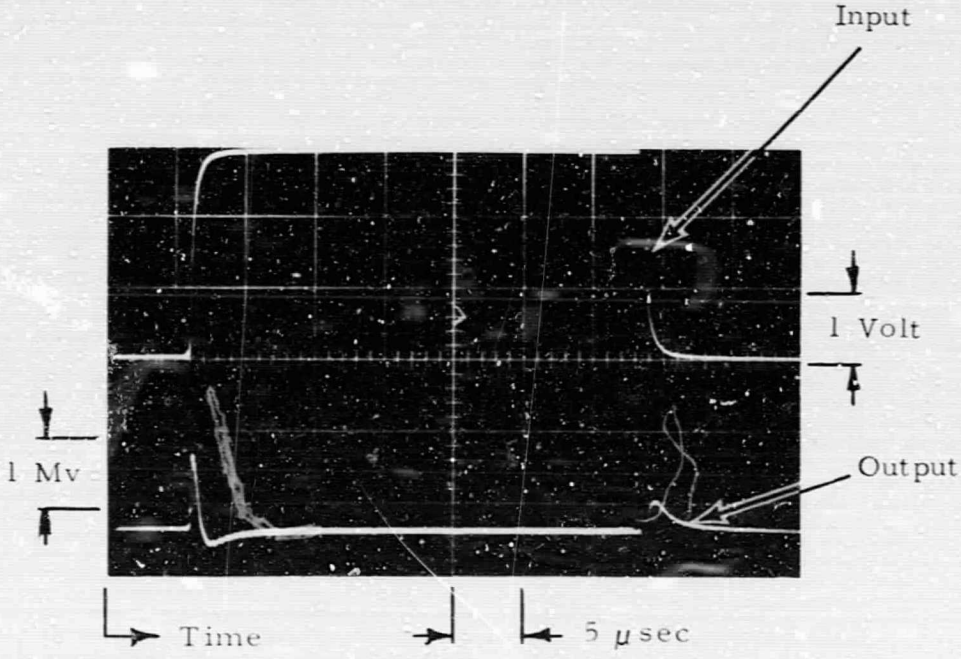

Figure 11b. Oscilloscope Traces of Input Calorimeter Gage Common Input and Residual Output.

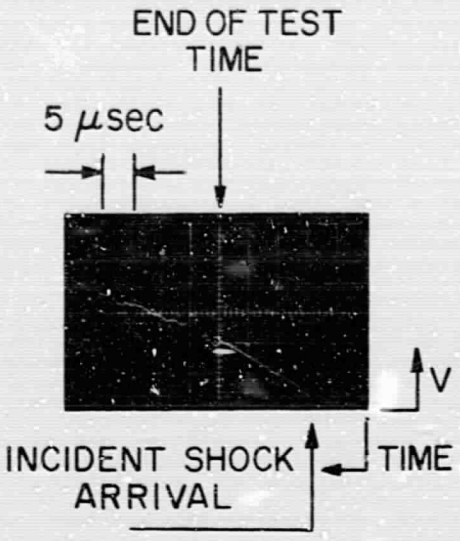

U_s = 27,900 FT./SEC. P_1 = 0.5 mm Hg

9 % CO_2 - 91 % N_2

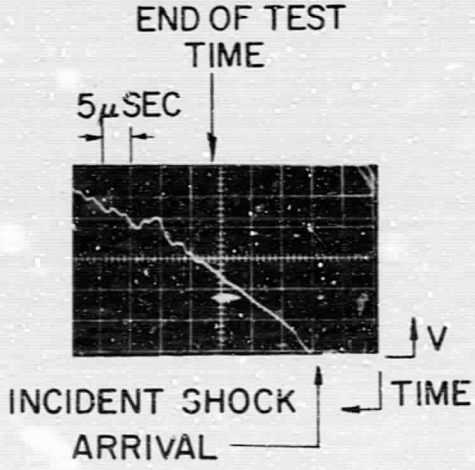

U_S = 31,000 FT/SEC P_1 = 0.5 mm Hg

25 % CO_2 - 75 % N_2

Figure 11c. Typical Traces of Stagnation Point Calorimeter Gage Signal.

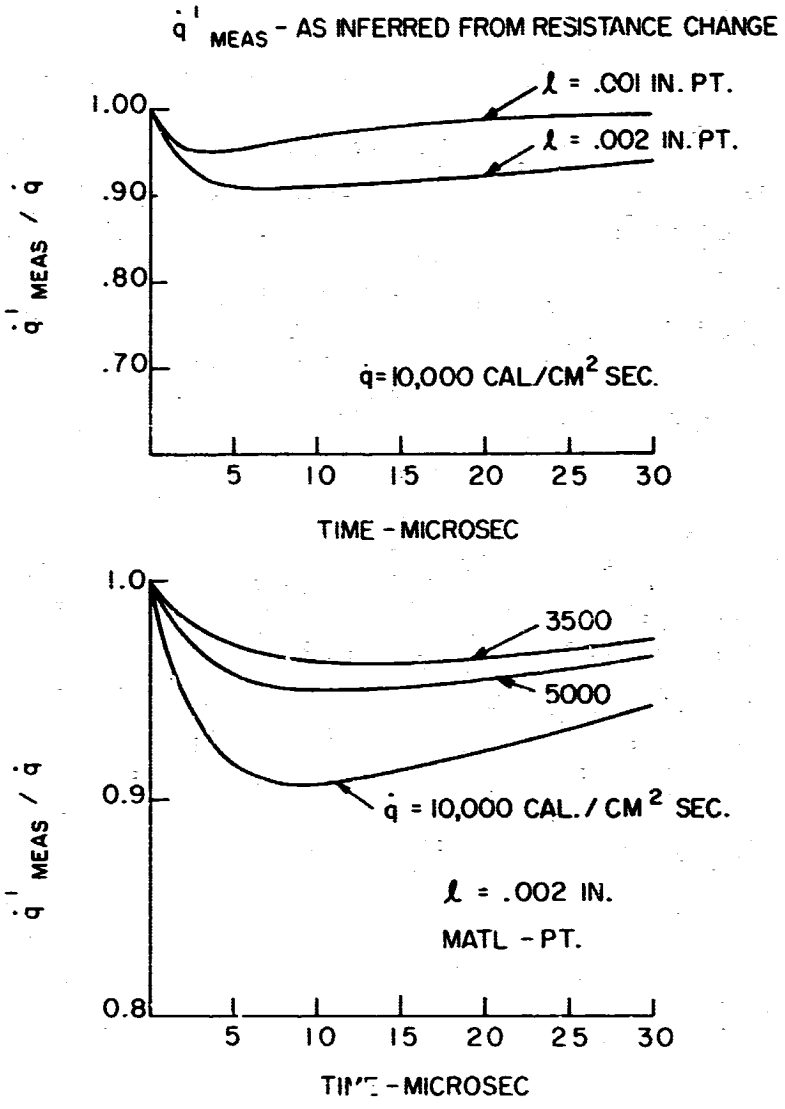

Figure 12. Theoretical Corrections for Platinum Calorimeter Heat Transfer Gages for Various Thickness and Heating Rates. Correction only for Temperature Distribution Effect and not for Losses to Backing Material.

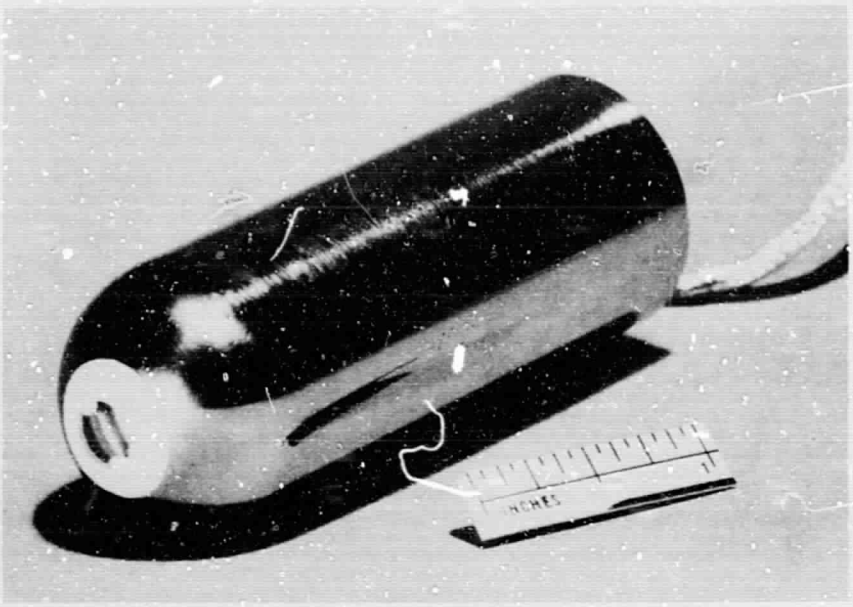

Figure 13a. Photograph of Thin Film Gage Model. Model $R_N = 0.5$ in.

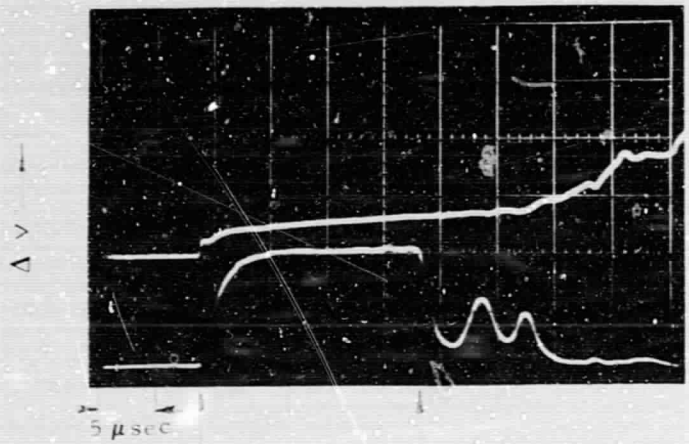

Figure 13b. Response of Stagnation Point Thin Film Heat Transfer Gage. Upper Trace - Heat Transfer Gage. Lower Trace - Sidewall Photomultiplier Viewing Shock Layer Ahead of Stagnation Point.

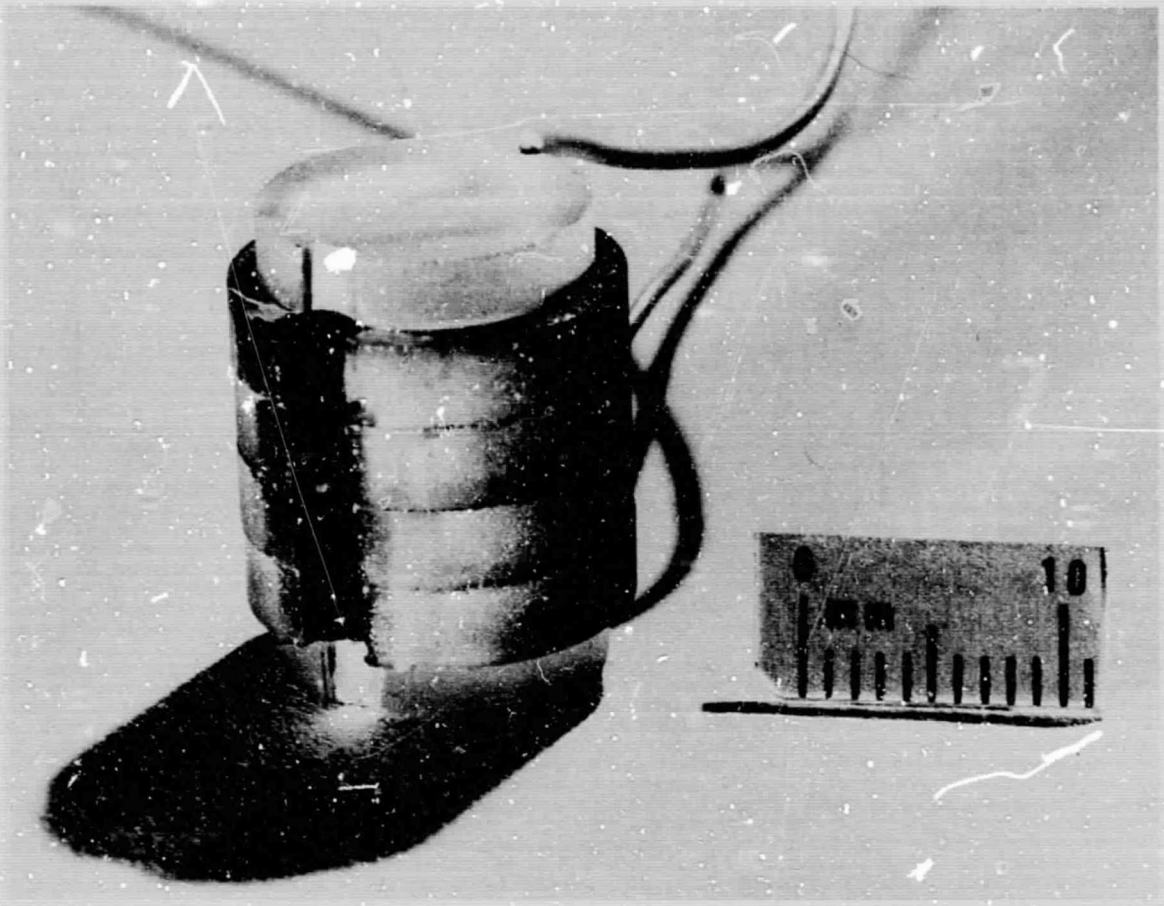

Figure 14a. Photograph of Cavity Gage.

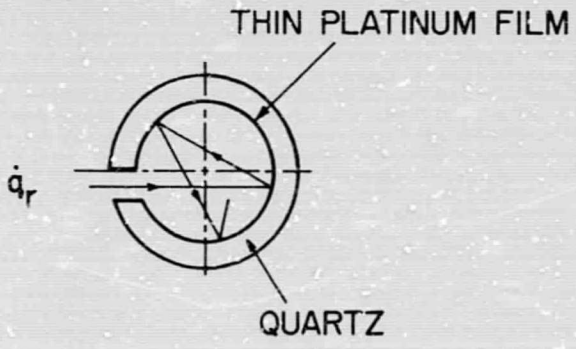

Figure 14b. Geometry of the Cylindrical Section.

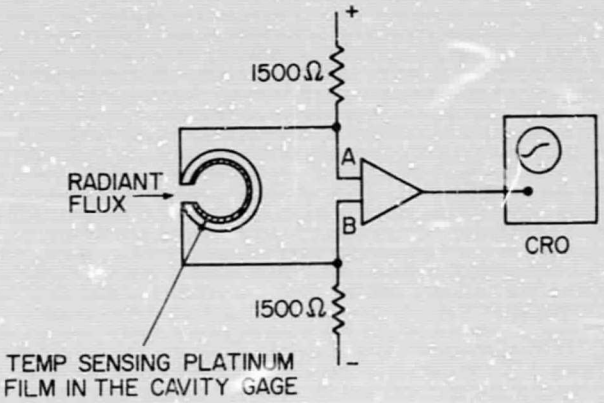

Figure 14c. Schematic Diagram of Cavity Gage Electrical Circuit.

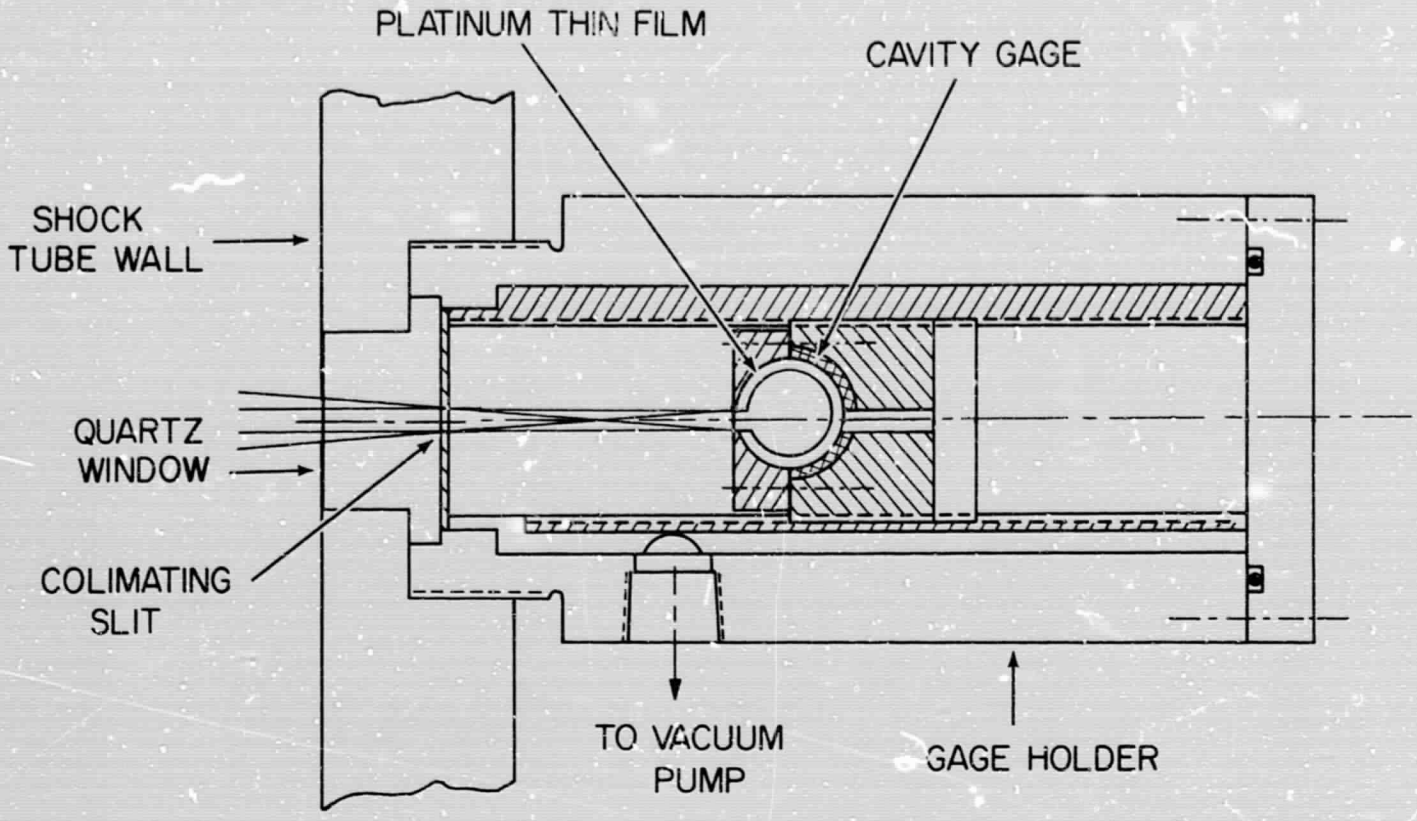

Figure 15a. Schematic Diagram of Total Radiation Cavity Gage in Sidewall Configuration.

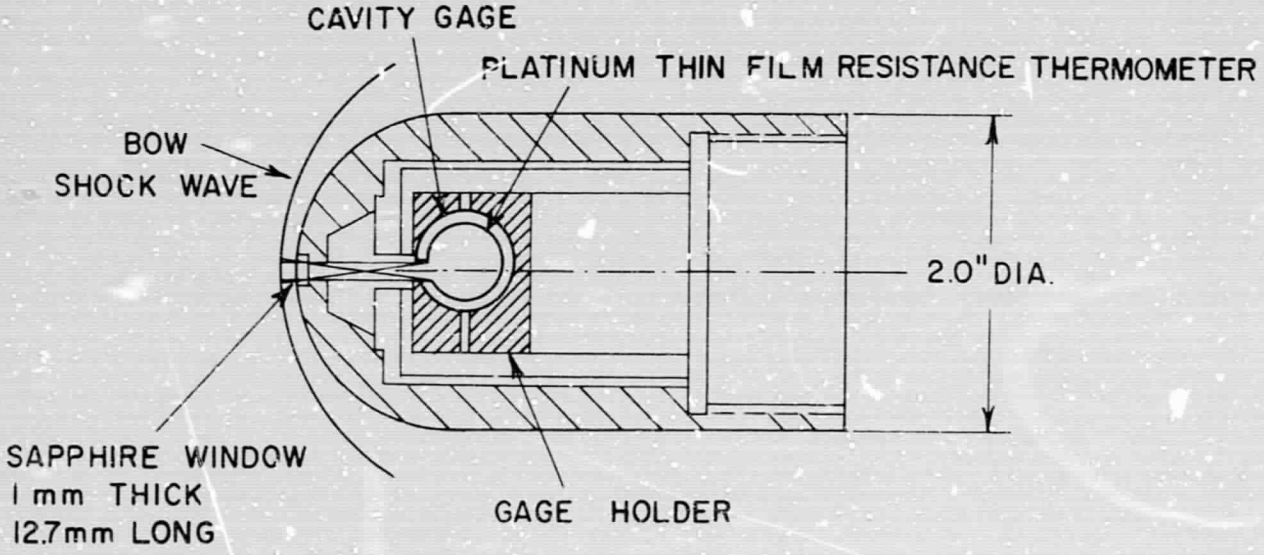

Figure 15b. Internal Model Arrangement of Stagnation Point Total Radiation Cavity Gage.

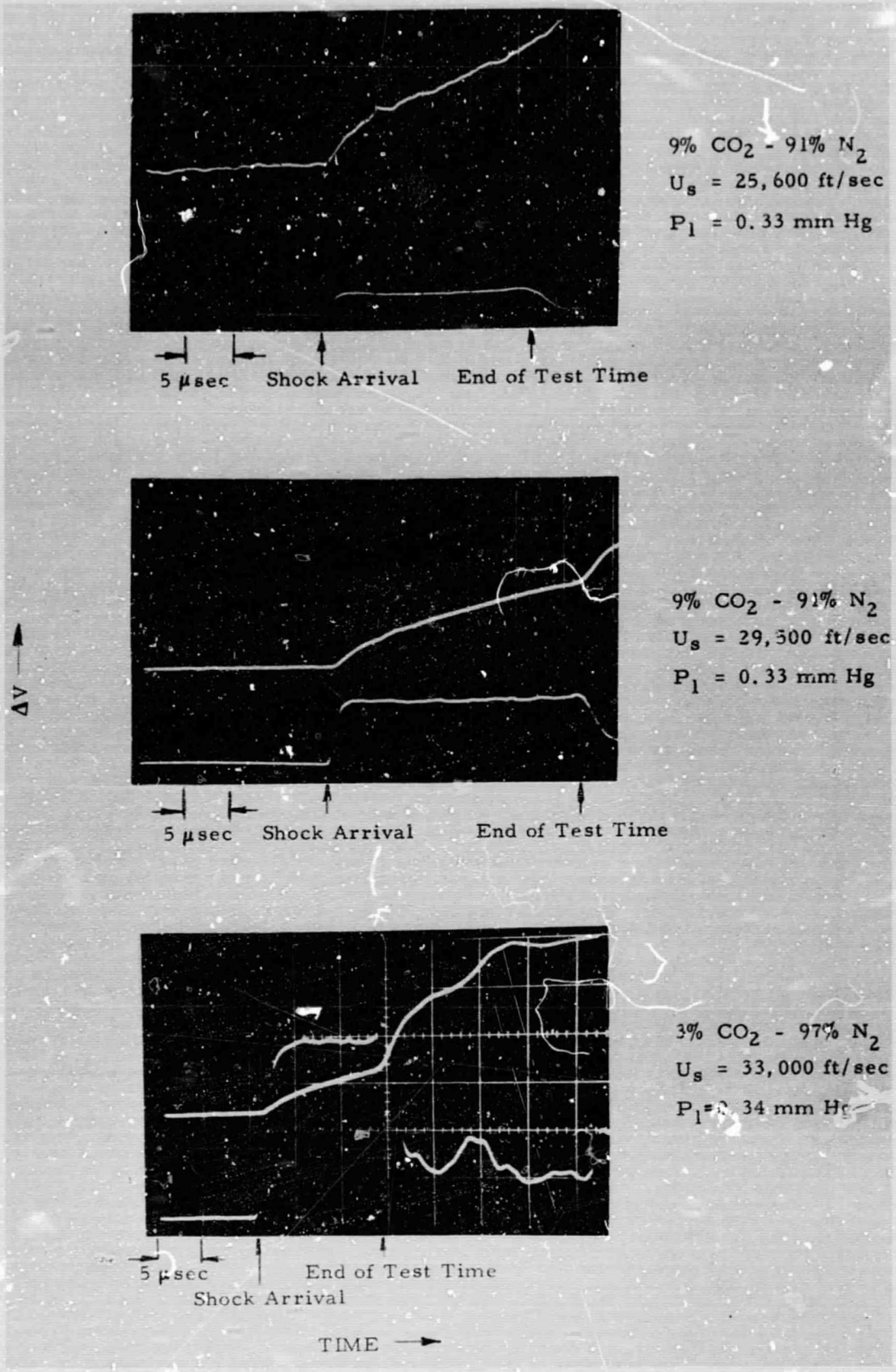

Figure 16. Oscilloscope Traces Showing Thin Film Cavity Gage Response During Test Gas Flow. Upper Trace - Model Stagnation Region Cavity Gage. Lower Trace - Sidewall Photomultiplier Sensitive in the Red Viewing Stagnation Region Shock Layer.

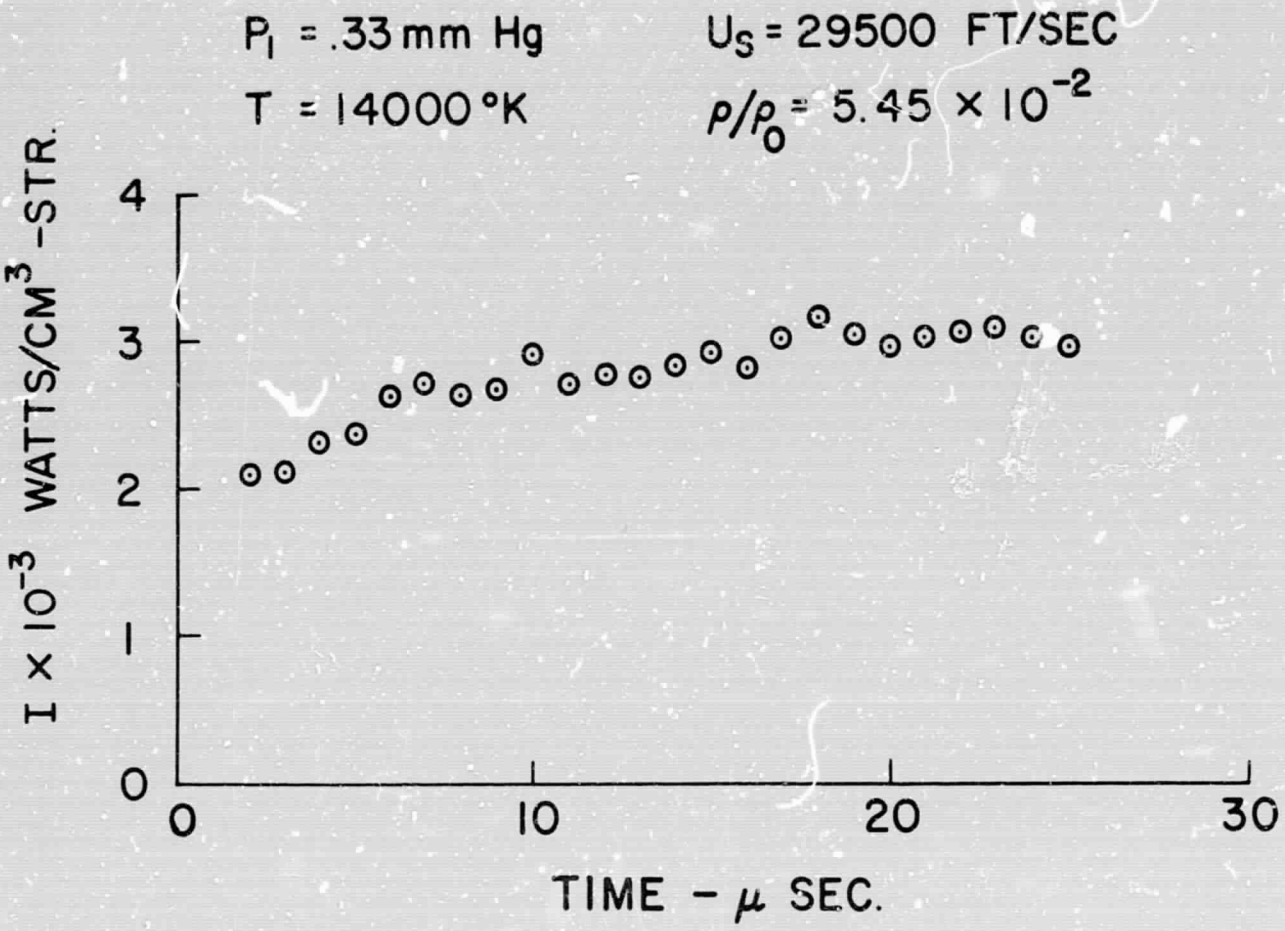

Figure 17. Radiance of Model Stagnation Region Gas as a Function of Time After Arrival of Incident Shock Wave at Model. Data Obtained from Analysis of Thin Film Cavity Gage Signal.